Supplementary Material for "Nonreciprocal Optomechanical Entanglement Against Backscattering Losses"

Ya-Feng Jiao,[1] Sheng-Dian Zhang,[1] Yan-Lei Zhang,[2,3] Adam Miranowicz,[4] Le-Man Kuang,[1,*] and Hui Jing[1,†]

[1]*Key Laboratory of Low-Dimensional Quantum Structures and Quantum Control of Ministry of Education, Department of Physics and Synergetic Innovation Center for Quantum Effects and Applications, Hunan Normal University, Changsha 410081, China*

[2]*CAS Key Laboratory of Quantum Information, University of Science and Technology of China, Hefei 230026, P. R. China*

[3]*CAS Center For Excellence in Quantum Information and Quantum Physics, University of Science and Technology of China, Hefei, Anhui 230026, P. R. China*

[4]*Faculty of Physics, Adam Mickiewicz University, 61-614 Poznań, Poland*

(Dated: September 1, 2020)

Here, we present the technical details on nonreciprocal optomechanical entanglement, including: (1) a summary of all parameter values used in our work; (2) experimental feasibility of our system, especially the conditions of stable coupling between the tapered fiber and the spinning resonator; (3) more discussions on mechanical or optical stability; (4) the influence of thermal effects and quality factors on nonreciprocal entanglement.

CONTENTS

S1. SYSTEM PARAMETERS

Table I shows the main symbols and parameters which have been used in this work.

Symbol	Definition	Name	Value
ω_m		Mechanical resonance frequency	63 MHz
γ_m		Mechanical linewidth	5.2 kHz
Q_m	ω_m/γ_m	Mechanical quality factor	1.21×10^4
T		Mechanical bath temperature	130 mK
n_m	$[\exp(\hbar\omega_m/k_B\mathrm{T})-1]^{-1}$	Thermal phonon occupation	269.4
m		Effective mass	10 ng
x_{zp}	$\sqrt{\hbar/(m\omega_m)}$	Zero point fluctuations	0.41 fm
ω_c		Optical resonance frequency	1.22 PHz
λ		Laser wavelength	1.55 μm
κ		Cavity linewidth	38.0 MHz
Q	ω_c/κ	Optical quality factor	3.2×10^7
P		Input laser power	20 mW or 100 mW
G_0	$\omega_c x_{\mathrm{zp}}/R$	Single-photon optomechanical coupling rate	452.1 Hz
R		Sphere radius	1.1 mm
r		Fiber radius	544 nm
Ω		Spinning frequency	8 kHz or 23 kHz
E		Young modulus of silica	75 GPa
Υ		Elastic limit of silica	9 GPa
ε_0		Dielectric constant of air	1
ε_1 (ε_2)		Dielectric constant of silica	3.9
n_0		Refractive index of air	1
n_1 (n_2)		Refractive index of silica	1.48

TABLE I. Feasible parameters. Unless specified otherwise, these parameters are applied to all evaluations in the text.

With these experimentally feasible parameters, we have confirmed that other quantum effects, such as two-mode squeezing or non-classicality, can also be manipulated in a highly asymmetric way in this optomechanical system, which may find applications in chiral quantum optics and technology [S1–S3].

S2. EXPERIMENTAL FEASIBILITY

A. Self-adjustment process

As shown in a very recent experiment [S4], we consider a whispering-gallery-mode silica sphere, which is mounted on a turbine and spins along its axis with, e.g., the angular velocity $\Omega = 6.6$ kHz for the sphere radius $r = 1.1$ mm. Faster rotations have also been reported in experiments by using, e.g., levitated nanomechanical rotors [S5, S6]. Then, by positioning the spinning resonator near a single-mode telecommunication fiber, light can be coupled into or out of the resonator evanescently.

For such a spinning device, the aerodynamic process plays a key role in the stable fiber-resonator coupling. Specifically, the fast spinning resonator can drag air into the region between the tapered fiber and the resonator, thereby forming a lubrication layer of air in this region. Then the thin film of air, exerting pressure on the surface of the tapered fiber facing the resonator, can make the fiber fly above the resonator with the separation of a few nanometres. Therefore, if any perturbation causes the taper to rise higher than the stable-equilibrium height, it can float back to its original position, which is referred to as “self-adjustment”.

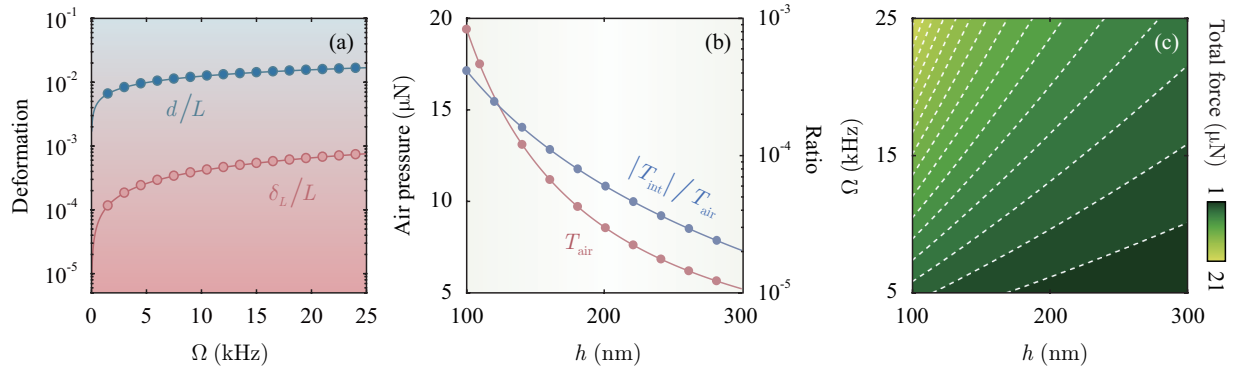

FIG. S1. Analysis of the "self-adjustment" behavior. (a) The strain ϵ (red curve) and the displacement d (blue curve) as a function of the angular velocity Ω for $h = 250\,\mathrm{nm}$. (b) The air pressure T_{air} and the ratio of intermolecular forces $|T_{\mathrm{int}}|/T_{\mathrm{air}}$ for varying taper-resonator separation h at $\Omega = 23\,\mathrm{kHz}$. (c) Total force between the fiber and the sphere versus the angular velocity Ω and the separation h. The resulting force of air pressure and intermolecular forces has a minimal value of $T_{\mathrm{tot}} = 1.135\,\mu\mathrm{N}$, which indicates the interactions of the fiber and the spinning sphere are always repulsive.

Hence the fiber will not touch or stick to the resonator even if it is pushed towards the spinning sphere [S4]. To see this clearly, we write the air pressure as $\Delta T_{\mathrm{air}} = (\rho\Delta\theta)T_{\mathrm{air}}/L$, with ρ (θ) the radius (angle) of the winding shape of the deformation region. Then, the total air pressure T_{air} on the taper can be estimated analytically as [S4]

$$T_{\mathrm{air}} = 6.19\mu R^{5/2}\Omega \int_0^r \left(h - \sqrt{r^2 - x^2} + r\right)^{-3/2} \mathrm{d}x, \tag{S2.1}$$

where μ is the viscosity of air, R (r) is the radius of the sphere (taper), and $h = h_0 + d$ represents the taper-resonator separation, with h_0 denoting the stationary gap between the fiber and the sphere. The local deformation can also lead to a tension on the infinitesimal cylinder of the fiber, which can be calculated by

$$\Delta T_{\mathrm{ela}} = 2\mathcal{F}\sin\left(\Delta\theta/2\right) \approx \mathcal{F}\Delta\theta, \tag{S2.2}$$

where $\mathcal{F}$ is the elastic force on the taper, obeying $\sigma = \mathcal{F}/(\pi r^2) = \epsilon \mathrm{E}$. Here σ is the uniaxial stress, E is the Young modulus of silica, and $\epsilon = \delta_L/L$ is the strain, where $\delta_L = L' - L$ denotes the variation of the original length L of the deformation region. Furthermore, δ_L can be straightforwardly derived via the following relations: $L' = \rho\theta$, $(L/2)^2 + (\rho - d)^2 = \rho^2$, and $\sin(\theta/2) = L/(2\rho)$. Hence, in the case of equilibrium (i.e., $\Delta T_{\mathrm{air}} = \Delta T_{\mathrm{ela}}$), T_{air} can be given in another form:

$$T_{\mathrm{air}} = 2\pi r^2 \mathrm{E}\left[\arcsin\left(\phi\right) - \phi\right] \approx \frac{\pi}{3} r^2 \phi^3 \mathrm{E}, \tag{S2.3}$$

where $\phi = 4Ld/\left(L^2 + 4d^2\right)$, and the approximation, $\arcsin(\phi) = \phi + \phi^3/6 + \cdots$, is made within the limit of $|\phi| \ll 1$, which physically requires a comparatively small distortion. As shown in Fig. S1(a), we confirmed that these approximation conditions can be easily satisfied with experimentally accessible parameters [S4, S7]: $\mathrm{E} = 75\,\mathrm{GPa}$, $r = 544\,\mathrm{nm}$, and $L = 3\,\mu\mathrm{m}$. In this case, the displacement d is given by

$$d = \frac{L}{2}\left(\beta - \sqrt{\beta^2 - 1}\right), \tag{S2.4}$$

where $\beta = \left[\pi r^2 \mathrm{E}/(3T_{\mathrm{air}})\right]^{1/3}$. The strain of the taper thus can be reduced to $\epsilon = \arcsin\left(\phi\right)/\phi - 1 \approx \phi^2/6$, from which we find that the strain (i.e., the elastic force) is positively associated with the taper-resonator separation:

$$\frac{\partial \mathcal{F}}{\partial h} = \pi r^2 \mathrm{E}\left(\frac{\partial \epsilon}{\partial d}\right) = \frac{16\pi r^2 \mathrm{E} L^2 d\left(L^2 - 4d^2\right)}{3\left(L^2 + 4d^2\right)^3} > 0. \tag{S2.5}$$

Equation (S2.5) clearly reveals that the elastic force becomes stronger when the air gap gets larger than the stable-equilibrium distance. Also, as shown in Fig. S1(b), the air pressure on the taper is largely suppressed. As a result, the taper can be dragged back to its original position when any perturbation causes it away from the spinning resonator, leading to the self-adjustment behavior. The self-adjustment of the tapered fiber enables the critical coupling of light into or out of the resonator, by which the counter-propagating beams can experience an optical drag identical in size, but opposite in sign.

B. Intermolecular forces

The intermolecular forces, such as the Casimir and van der Waals forces, could also affect the stable fiber-resonator coupling. In our system, such kinds of intermolecular forces can be described as [S4]:

$$T_{\rm int} = rR\left(-\frac{\mathbb{A}}{6\pi h^3} + \frac{\mathbb{B}}{45\pi h^9} - \frac{\pi^2 c\hbar}{240h^4}\right), \tag{S2.6}$$

where the Hamaker constant $\mathbb{A}$ can be calculated by [S8]:

$$\mathbb{A} = \frac{3\varepsilon_-^{(1)}\varepsilon_-^{(2)}k_{\rm B}{\rm T}}{4\varepsilon_+^{(1)}\varepsilon_+^{(2)}} + \frac{\nu\left[n_-^{(1)}n_-^{(2)}\right]^2}{n_+^{(1)}n_+^{(2)}\left[n_+^{(1)}+n_+^{(2)}\right]}, \tag{S2.7}$$

with $\nu = 3\sqrt{2}\hbar\nu_e/16$, $\varepsilon_\pm^{(u)} = \varepsilon_u \pm \varepsilon_0$, $n_\pm^{(u)} = \sqrt{n_u^2 \pm n_0^2}$, and $u = 1, 2$. Hereafter, we use ε_0 (n_0), ε_1 (n_1), and ε_2 (n_2) to represent the dielectric constant (the refractive index) of the air, the taper and the spinning resonator, respectively; $k_{\rm B}$ is the Boltzmann constant, T is the mechanical bath temperature, and $\nu_e = 3\,{\rm PHz}$ [S8]. Note that for simplicity, we have replaced n_2 with n in the main text. Moreover, the constant $\mathbb{B}$ is typically of the order of $10^{-76}\ {\rm J\,m^6}$ for interactions between condensed matter phases across the vacuum or air [S9]. Taking intermolecular forces into account, the total force between the taper and the resonator becomes: $T_{\rm tot} = T_{\rm air} + T_{\rm int}$. Herein, we choose experimentally accessible parameters [S10]: $\varepsilon_0 = 1$, $\varepsilon_1 = \varepsilon_2 = 3.9$, $n_0 = 1$, $n_1 = n_2 = 1.48$, and ${\rm T} = 130\,{\rm mK}$. As expected, the intermolecular forces are found to be negligible ($< 0.1\%$), and the taper-resonator interactions remain repulsive [see Figs. S1(b) and S1(c)]. Thus, the effects of the Casimir and van der Waals forces can be safely omitted on critical coupling. Other factors, such as lubricant compressibility, tapered-fiber stiffness, and the wrap angle of a fiber, may also affect critical coupling. However, these factors are confirmed to be negligible in experiments, which can be also safely ignored in our discussions [S4].

S3. STABILITY CONDITIONS

A. Mechanical stability

The realization of stable fiber-resonator coupling sets a limit to the angular velocity of spinning devices. Specifically, the requirement $\beta \geq 1$ in Eq. (S2.4) yields the first limit:

$$\Omega_0 = \frac{\varrho\pi r^2{\rm E}}{18.57\mu R^{5/2}}, \tag{S3.8}$$

where

$$\varrho = \left[\int_0^r \left(h - \sqrt{r^2-x^2} + r\right)^{-3/2}{\rm d}x\right]^{-1}. \tag{S3.9}$$

Also, the tiny displacement should obey $d = h - h_0 < h$, which gives the second limit:

$$\Omega_1 = \frac{\varrho\pi r^2\Lambda{\rm E}}{18.57\mu R^{5/2}}, \tag{S3.10}$$

where $\Lambda = \left[4Lh/\left(L^2+4h^2\right)\right]^3$. Finally, the elastic limit of the tapered fiber provides the third stability condition ($\sigma = \Upsilon$):

$$\Omega_2 = \frac{\varrho\pi r^2\Upsilon}{3.095\mu R^{5/2}}\sqrt{\frac{6\Upsilon}{\rm E}}, \tag{S3.11}$$

where Υ is typically $9\,{\rm GPa}$ for silica devices [S11]. Thus, the mechanical limit to the angular velocity can be obtained as:

$$\Omega_{\rm max} = \min\left\{\Omega_0, \Omega_1, \Omega_2\right\}. \tag{S3.12}$$

When operating at taper-resonator separations near $250\,{\rm nm}$, we have $\Omega_0 = 81.6\,{\rm MHz}$, $\Omega_1 = 2.8\,{\rm MHz}$, $\Omega_2 = 49.9\,{\rm MHz}$, and thus $\Omega_{\rm max} = 2.8\,{\rm MHz}$. Therefore, it is reasonable to use $\Omega = 8\,{\rm kHz}$ or $23\,{\rm kHz}$ in the main text.

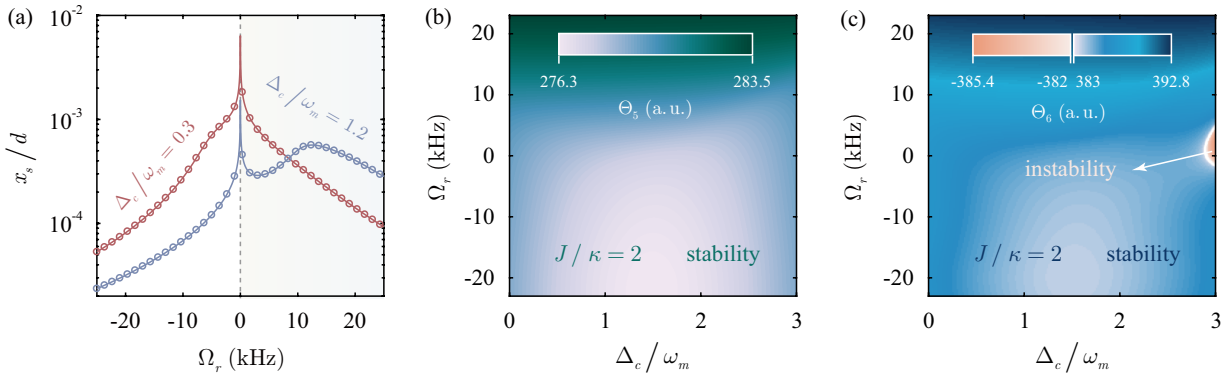

FIG. S2. The mechanical and optical stability conditions. (a) The ratio of the mean mechanical displacement x_s to the air-induced displacement d as a function of the angular velocity Ω_r. In the aerodynamic process, this ratio is extremely small ($\sim 0.1\%$), meaning that radial breathing of the resonator is negligible compared to the air-induced displacement. (b-c) Stability functions Θ_5 and Θ_6 versus the angular velocity Ω_r and the scaled optical detuning Δ_c/ω_m at $J/\kappa = 2$ and $P = 20\,\mathrm{mW}$. The white contour line in (c) is the boundary between the stability and instability regions, and a.u. denotes arbitrary units. The parameters are listed in Table I.

Moreover, we also consider the influence of the radial breathing of the resonator on stable fiber-resonator coupling. In paticular, we compare the mean mechanical displacement x_s with the air-induced displacement d, i.e.,

$$\eta = x_s/d = q_s x_{\mathrm{zp}}/d, \tag{S3.13}$$

where $x_{\mathrm{zp}} = \sqrt{\hbar/(m\omega_m)}$ denotes the standard deviation of the zero-point motion of the mechanical mode. As shown in Fig. S2(a), the effect of the mechanical displacement is negligible indeed ($< 1\%$), thereby the radial breathing of the resonator does not disturb the critical evanescent coupling. Note that, for simplicity, we have introduced $\Omega_r = \pm\Omega$.

B. Optical stability

According to Routh-Hurwitz criterion [S12], the system is stable and reaches its steady state when all eigenvalues of the matrix A have negative real parts. Therefore, we start our analysis by determining the eigenvalues of the matrix A, i.e., $|A - \lambda I| = 0$, yielding the following characteristic equation:

$$\lambda^6 + a_1\lambda^5 + a_2\lambda^4 + a_3\lambda^3 + a_4\lambda^2 + a_5\lambda + a_6 = 0, \tag{S3.14}$$

where

$$\begin{aligned}
&a_1 = 4\kappa + \gamma_m, \quad a_2 = \sigma_0 + \omega_m^2 + 4\kappa(\kappa + \gamma_m),\\
&a_3 = \sigma_0(2\kappa + \gamma_m) + 4\kappa\left(\omega_m^2 + \kappa\gamma_m\right), \quad a_4 = \sigma_0\sigma_1 + \sigma_2 + 4\kappa^2\omega_m^2,\\
&a_5 = \gamma_m\mu_2 - 2\kappa\mu_0\mu_3\left(\gamma_m\mu_0 + 4\kappa\omega_m^2\right) + \kappa\mu_1\left(\kappa\gamma_m + 2\omega_m^2\right),\\
&a_6 = \omega_m\left(\sigma_+ + \sigma_- + \sigma_2\omega_m - \mu_0\mu_4\right) - \mu_3\tilde{\Delta}_+\tilde{\Delta}_-,
\end{aligned} \tag{S3.15}$$

and

$$\begin{aligned}
&\sigma_0 = 2\mu_0 + \mu_1, \quad \sigma_1 = \kappa^2 + 2\kappa\gamma_m + \omega_m^2, \quad \sigma_2 = \mu_0^2 + \kappa^2\mu_1 + \mu_2,\\
&\sigma_2 = \mu_2 - \mu_3 + \mu_0\left(J^2 - \kappa^2\right), \quad \sigma_\pm = (\Delta_\pm J^2 - \Delta_\mp\kappa^2)G_\mp^2,\\
&\mu_0 = J^2 + \kappa^2, \quad \mu_1 = \tilde{\Delta}_+^2 + \tilde{\Delta}_-^2, \quad \mu_2 = (\tilde{\Delta}_+\tilde{\Delta}_- - 2J^2)\tilde{\Delta}_+\tilde{\Delta}_-,\\
&\mu_3 = \omega_m(\tilde{\Delta}_+|G_{\circlearrowleft}|^2 + \tilde{\Delta}_-|G_{\circlearrowleft}|^2 + \mu_4), \quad \mu_4 = 2J(G_{\circlearrowleft}^x G_{\circlearrowleft}^x + G_{\circlearrowleft}^y G_{\circlearrowleft}^y).
\end{aligned} \tag{S3.16}$$

Using the coefficients a_k, we can form a set of $k \times k$ matrices, θ_k, for $k \le 6$, with their entries defined as:

$$\theta_{ln} = \begin{cases} 0, & 2l - n < 0 \text{ or } 2l - n > k,\\ a_{2l-n}, & \text{otherwise.} \end{cases} \tag{S3.17}$$

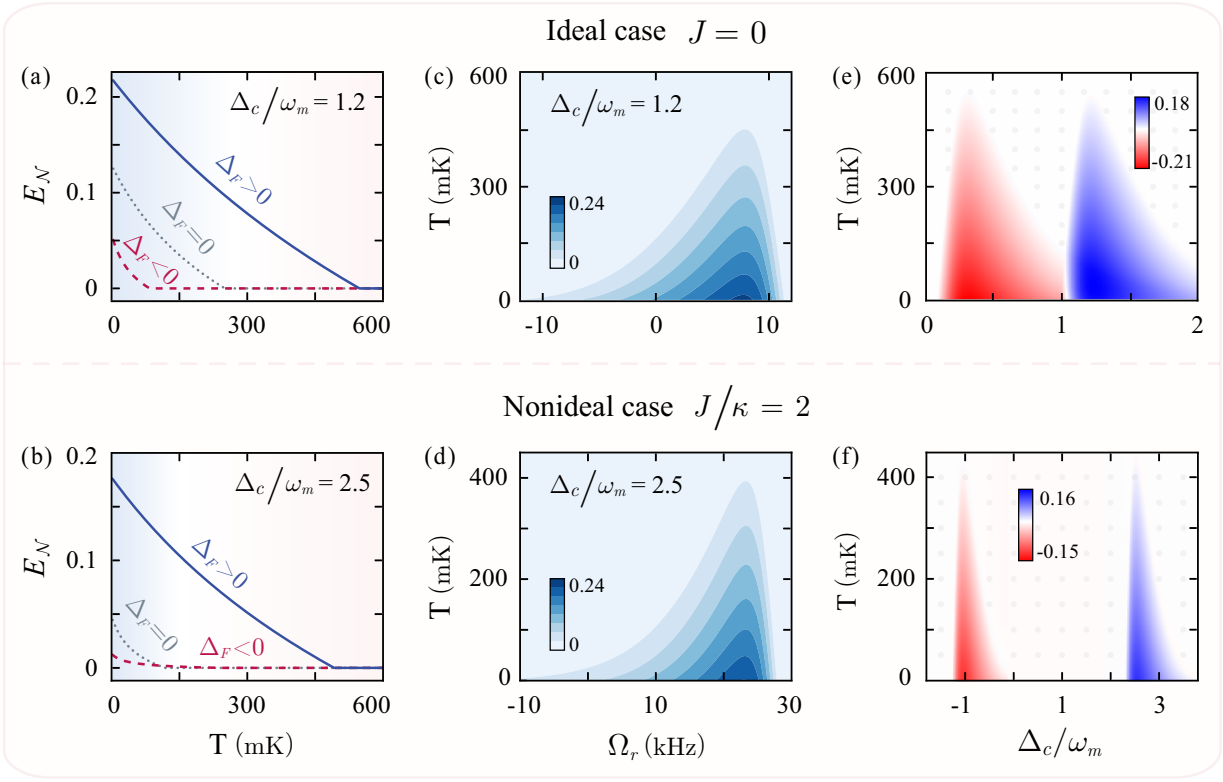

FIG. S3. Thermal effect on nonreciprocal optomechanical entanglement. (a-b) The logarithmic negativity $E_\mathcal{N}$ as a function of the environment temperature T for different driving directions. (c-d) Density plot of the logarithmic negativity $E_\mathcal{N}$ versus the angular velocity Ω_r and the environment temperature T. (e-f) The COM entanglement difference with respect to different driving directions, $\Delta E_\mathcal{N}$, versus the scaled optical detuning Δ_c/ω_m and the environment temperature T. The rotation speed is chosen as $\Omega = 8\,\text{kHz}$ in (a) and (e), and $\Omega = 23\,\text{kHz}$ in (b) and (f). Other parameters are listed in Table I.

The stability conditions can be satisfied when all the determinants of the matrices θ_k are positive [S12]. Through careful analysis, we find only θ_5 and θ_6 are nontrivial. As shown in Figs. S2(b) and S2(c), we numerically plot these functions in a logarithmic form, i.e.,

$$\Theta_k = \begin{cases} \ln \theta_k, & \theta_k > 0, \\ -\ln |\theta_k|, & \theta_k < 0. \end{cases} \tag{S3.18}$$

Note that θ_k and Θ_k maintain the same sign within the parameters used in the main text, thus the contour line in Fig. S2(c) clearly determines the boundary between the stability and instability regions. In this case, we can confirm that these experimentally feasible parameters keep this optomechanical system in a stable zone.

S4. THE ROLE OF THERMAL EFFECTS AND QUALITY FACTORS

Thermal noises can destroy fragile quantum correlations in practical devices. Thus protecting quantum resources from environmental thermal perturbations is essential for achieving quantum nonreciprocity. To see the influence of the thermal effect on nonreciprocal optomechanical entanglement, we plot the logarithmic negativity $E_\mathcal{N}$ with respect to the environment temperature T in Figs. S3(a) - S3(d). We find that nonreciprocal optomechanical entanglement in a chosen direction can exist at higher temperature compared to the case of a stationary system. This means that, by spinning the resonator, optomechanical entanglement can be more robust against thermal noises. In addition, by defining the difference of COM entanglement for the opposite driving directions: $\Delta E_\mathcal{N} \equiv E_{\mathcal{N},\circlearrowleft} - E_{\mathcal{N},\circlearrowright}$, we demonstrate the dependence of quantum nonreciprocity on environmental temperature in Figs. S3(e) and S3(f). Clearly, the condition $\Delta E_\mathcal{N} \neq 0$ can be satisfied even at $\text{T} \sim 600\,\text{mK}$. Thereby, quantum nonreciprocity provides a new strategy to protect quantum entanglement in a noisy environment, i.e., enhancing the entanglement quality in a chosen (wanted) direction at the price of losing its quality in the other (unwanted) direction. This new possibility, as far as we know, has not been revealed in all previous works.

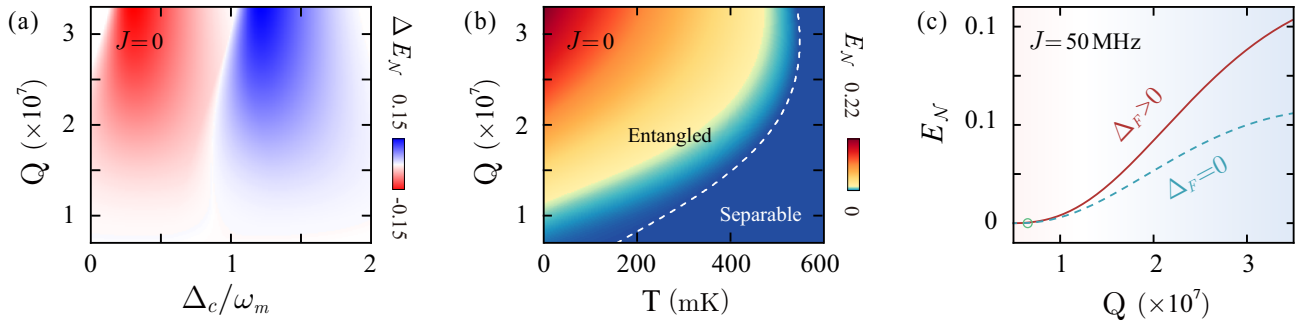

FIG. S4. The influence of Q-factor on nonreciprocal optomechanical entanglement. (a) The COM entanglement difference, $\Delta E_{\mathcal{N}}$, versus the scaled optical detuning Δ_c/ω_m and the quality factor Q at temperature T $= 130$ mK. (b) Density plot of the logarithmic negativity $E_{\mathcal{N}}$ versus the environment temperature T and the quality factor Q at $\Delta_c/\omega_m = 1.2$. (c) The logarithmic negativity $E_{\mathcal{N}}$ as a function of the quality factor Q at $\Delta_c/\omega_m = 1.6$. The rotation speed is chosen as $\Omega = 8$ kHz in (a)-(c). Other parameters are listed in Table I.

In addition, the Q-factor of the resonator also affects the realization of quantum nonreciprocity. In case of $J = 0$, as shown in Fig. S4(a), it is found that quantum nonreciprocity can persist for $Q \geq 10^7$ at T $= 130$ mK but its degree is lowered by decreasing the values of Q. Fig. S4(b) shows that both lower Q-factor and higher temperature are harmful for the robustness of COM entanglement. In addition, it is seen that COM entanglement even completely vanishes at high temperatures regardless of Q-factors. Moreover, in the presence of backscattering, e.g., $J = 50$ MHz, it is found that for the same values of Q and T, by spinning the resonator, nonreciprocal entanglement can always be better than that in a nonspinning device [see Fig. S4(c)]. These results indicate that considerable entanglement revival can be achieved with high Q-factor spinning resonators.

* lmkuang@hunnu.edu.cn
† jinghui73@gmail.com

[S1] P. Lodahl, S. Mahmoodian, S. Stobbe, A. Rauschenbeutel, P. Schneeweiss, J. Volz, H. Pichler, and P. Zoller, Chiral quantum optics, Nature (London) **541**, 473 (2017).
[S2] H. J. Kimble, The quantum internet, Nature (London) **453**, 1023 (2008).
[S3] K. Stannigel, P. Komar, S. J. M. Habraken, S. D. Bennett, M. D. Lukin, P. Zoller, and P. Rabl, Optomechanical Quantum Information Processing with Photons and Phonons, Phys. Rev. Lett. **109**, 013603 (2012).
[S4] S. Maayani, R. Dahan, Y. Kligerman, E. Moses, A. U. Hassan, H. Jing, F. Nori, D. N. Christodoulides, and T. Carmon, Flying couplers above spinning resonators generate irreversible refraction, Nature (London) **558**, 569 (2018).
[S5] R. Reimann, M. Doderer, E. Hebestreit, R. Diehl, M. Frimmer, D. Windey, F. Tebbenjohanns, and L. Novotny, GHz Rotation of an Optically Trapped Nanoparticle in Vacuum, Phys. Rev. Lett. **121**, 033602 (2018).
[S6] J. Ahn, Z. Xu, J. Bang, Y.-H. Deng, T. M. Hoang, Q. Han, R.-M. Ma, and T. Li, Optically Levitated Nanodumbbell Torsion Balance and GHz Nanomechanical Rotor, Phys. Rev. Lett. **121**, 033603 (2018).
[S7] Y. Bellouard, A. A. Said, and P. Bado, Opt. Express **13**, 6635 (2005).
[S8] J. Chen, G. Zhou, L. Zhang, and W. Sun, Influence of Intermolecular Force on the Head-Disk Interface of HDD with High Recording Density, in *2009 Symposium on Photonics and Optoelectronics* (IEEE, 2009) pp. 1-4.
[S9] L. Wu and D. B. Bogy, Effect of the Intermolecular Forces on the Flying Attitude of Sub-5 NM Flying Height Air Bearing Sliders in Hard Disk Drives, J. Tribol. **124**, 562 (2002).
[S10] R. J. Joyce, H. F. Sterling, and J. H. Alexander, Silicon oxide and nitride films deposited by an r.f. glow-discharge, Thin Solid Films **1**, 481 (1968).
[S11] H. Sugiura, R. Ikeda, K. Kondo, and T. Yamadaya, Densified silica glass after shock compression, J. Appl. Phys. **81**, 1651 (1997).
[S12] E. X. DeJesus and C. Kaufman, Routh-Hurwitz criterion in the examination of eigenvalues of a system of nonlinear ordinary differential equations, Phys. Rev. A **35**, 5288 (1987).